UPPSALA
UNIVERSITET

Magnetic Divergence Cleaning in Magnetohydrodynamics

David Niemelä, Matilda Tiberg, Anton Waltgård

Project in Computational Science: Report

February 2022
Supervisors: Tuan Anh Dao, Lukas Lundgren

PROJECT REPORT

Institutionen för informationsteknologi

Abstract

We compare different divergence cleaning methods for imposing the physically relevant condition $\nabla \cdot \mathbf{B} = 0$ when solving the magnetohydrodynamic equations. Projection, Pseudo time-stepping, Generalized Lagrange Multiplier, Artificial Compressibility and Grad-div stabilization are the divergence cleaning methods that are examined. The methods are implemented with a robust high-order shock capturing solver and are compared for three different benchmarks. All methods achieve the expected convergence rate for a smooth problem, and all methods are capable of reducing the divergence in discontinuous shock-filled problems such as the Orszag-Tang vortex problem. The numerical results show that the Artificial Compressibility method combined with Grad-div stabilization with properly chosen parameter values best enforce the divergence free condition.

Contents

1 Introductionon **1**
- 1.1 Background . . . 1
- 1.2 Objective . . . 1
- 1.3 Implementation . . . 1

2 The Magnetohydrodynamic Equations **1**
- 2.1 Divergence Free Condition . . . 2

3 Galerkin Finite Element Method **2**
- 3.1 Taylor-Hood Element . . . 3
- 3.2 Time Discretization . . . 3

4 Divergence Cleaning Methods **4**
- 4.1 Projection . . . 4
- 4.2 Pseudo-Timestepping . . . 4
- 4.3 Generalized Lagrange Multipliers . . . 5
- 4.4 Artificial Compressibility . . . 5
- 4.5 Grad-Div Stabilization . . . 5

5 Numerical Benchmarks **6**
- 5.1 Smooth Vortex Problem[15] . . . 6
- 5.2 2D Orszag-Tang[13] . . . 6
- 5.3 Cylinder Flow . . . 6
  - 5.3.1 Boundary conditions . . . 7

6 Results **7**
- 6.1 Smooth Vortex Problem . . . 7
- 6.2 2D Orszag-Tang . . . 7
  - 6.2.1 $\mathbb{P}_1$ Discretization . . . 8
  - 6.2.2 $\mathbb{P}_2$ Discretization . . . 9
  - 6.2.3 Taylor-Hood Discretization . . . 9
  - 6.2.4 Summary . . . 10
- 6.3 Cylinder Flow . . . 11

7 Conclusions **12**

Appendix A - Convergence Tables: Smooth Vortex Problem **14**

Appendix B - AC Penalty Parameter **18**

1 Introductionon

1.1 Background

The magnetohydrodynamic (MHD) equations are first constructed by Hannes Alfvén and constitute a system of conservation laws that describes the behavior of a conducting fluid in the presence of a magnetic field. An example of such a system is the sun, which consists of plasma. The derivation is made by combining the Euler and Maxwell's equations. For this work Alvfén has been awarded the Nobel prize in Physics in year 1970 [1].

The Euler equation describes the ideal flow of a fluid. When the fluid attains a high enough temperature (energy), it turns into plasma which is an ionized gas. To model this, the magnetic field is added to the Euler system, and thus the MHD equations are attained. When the gas reaches high speed flows, there occur shocks, which is a phenomenon that traditionally is hard to capture with finite element methods (FEM). This requires to introduce stabilization methods, as is done in [6].

One reason why the research field in divergence cleaning methods is of importance is due to the fact that when too much divergence is introduced into the system, the solutions quickly become non-physical and often explode. This could be due to discontinuities which leads to negative density. If the density becomes negative, then all physics breaks down (entropy principle is being destroyed) and the solution explodes.

1.2 Objective

The purpose with the project is to evaluate several different cleaning methods applied to the MHD equations, namely specific discretization techniques in order to lower the magnetic divergence in the standard FEM setting. These techniques are then applied on three different benchmarks: a smooth problem with analytical solution, Orszag-Tang (non-smooth) and cylinder flow. For one of the evaluated cleaning methods, there exists a tunable parameter value that highly affects the results. Hence, a part of this project focuses on finding a suitable parameter value that fulfills certain requirements when applied to the Orszag-Tang benchmark. In the cylinder flow problem, different boundaries are imposed and evaluated.

1.3 Implementation

FEniCS is an open source computing platform for solving partial differential equations (PDE:s) discretized by FEM, and is used for examining the different cleaning methods. The implementation of the different divergence cleaning methods is based on an already existing software library that implements the basic MHD equations in FEniCS. The code is written in both C++ and Python.

2 The Magnetohydrodynamic Equations

The governing equations of the ideal conservative MHD-system are presented in (1a-d), where *ideal* refers to when the resistive and viscous effects of the fluids can be ignored. In this report, a dimensionless form is used for the MHD equations. The system of equations to be solved reads as follows,

$$\partial_t \rho + \nabla \cdot \mathbf{m} = 0, \tag{1a}$$
$$\partial_t \mathbf{m} + \nabla \cdot (\mathbf{m} \otimes \mathbf{u} + p\mathbf{I}) + \nabla \cdot (-\beta) = 0, \tag{1b}$$
$$\partial_t E + \nabla \cdot (E + p) + \nabla \cdot (-\mathbf{u} \cdot \beta) = 0, \tag{1c}$$
$$\partial_t \mathbf{B} + \nabla \cdot (\mathbf{u} \otimes \mathbf{B} - \mathbf{B} \otimes \mathbf{u}) = 0. \tag{1d}$$

The physical equivalents of the equations are: (1a) conservation of mass, (1b) is the conservation of momentum, (1c) conservation of energy and (1d) comes from Faraday's law[14].

The system is defined on the spatial domain $\Omega \in \mathbb{R}^d$, where d denotes the spatial dimension, and on the time interval as $t \in [0,\ T]$ where T is the final time. The MHD equations are simulated on a two dimensional

(2D) domain, hence $d = 2$ is used throughout this report. The equations consists of the mass density $\rho \in \mathbb{R}$, the total energy of the system $E \in \mathbb{R}$, the momentum $\mathbf{m} \in \mathbb{R}^d$ and the magnetic field $\mathbf{B} \in \mathbb{R}^d$.

The variable p in (1b) and (1c) is the thermodynamic pressure and is calculated as $p = (\gamma - 1)e$, where γ is the adiabatic constant and the internal energy e is given by $e = E - \frac{1}{2}\rho(\mathbf{u} \cdot \mathbf{u}) - \frac{1}{2}(\mathbf{B} \cdot \mathbf{B})$. The term $\mathbf{u}$ is the velocity field, $\mathbf{u} = \mathbf{m}/\rho$, and β is Maxwell's stress tensor given by

$$\beta = \left(-\frac{1}{2} (\mathbf{B} \cdot \mathbf{B}) \mathbf{I} + \mathbf{B} \otimes \mathbf{B} \right).$$

where $\mathbf{I}$ is the identity matrix of size $d \times d$ [5]. To demonstrate the combination of fluid dynamic and electromagnetic properties, the system of equations (1) can be rewritten in the form:

$$\partial_t \mathbf{U} + \nabla \cdot \mathbf{F}_\varepsilon(\mathbf{U}) + \nabla \cdot \mathbf{F}_\mathcal{B}(\mathbf{U}) = \mathbf{0},$$

$$\mathbf{F}_\varepsilon := \begin{bmatrix} \mathbf{m} \\ \mathbf{m} \otimes \mathbf{u} + p\mathbf{I}, \\ \mathbf{u}(E + p) \\ 0 \end{bmatrix} \qquad \mathbf{F}_\mathcal{B} := \begin{bmatrix} 0 \\ -\beta \\ -\mathbf{u} \cdot \beta \\ \mathbf{u} \otimes \mathbf{B} - \mathbf{B} \otimes \mathbf{u} \end{bmatrix},$$

where the solution vector is denoted by $\mathbf{U} = [\rho,\ \mathbf{m},\ E,\ \mathbf{B}]^T$. The eigenvalues for the MHD have the following form:

$$\lambda_{1,8} = \mathbf{u} \cdot \mathbf{e} \mp c_f, \quad \lambda_{2,7} = \mathbf{u} \cdot \mathbf{e} \mp b, \quad \lambda_{3,6} = \mathbf{u} \cdot \mathbf{e} \mp c_s, \quad \lambda_{4,5} = \mathbf{u} \cdot \mathbf{e} \tag{2}$$

The variables c_f and c_s refer to fast and slow magnetosonic waves respectively, where the expression for these waves is given in [5]. The direction vector is denoted by $\mathbf{e} \in \mathbb{R}^2$ and the variable $b := \mathbf{B} \cdot \mathbf{e}/\sqrt{\rho}$. It can be concluded that the largest absolute value of the eigenvalues are given by $\lambda_{1,8}$, and will later be referred to as maximum wave speed.

2.1 Divergence Free Condition

According to Maxwell's equations, the magnetic field $\mathbf{B}$ is the curl of an electric field. Combined with the vector identity $\nabla \cdot (\nabla \times \bullet) = 0$, we obtain a condition for the divergence of the $\mathbf{B}$-field to be zero, which is necessary for mathematical consistency, namely,

$$\nabla \cdot \mathbf{B} = 0. \tag{3}$$

Discretizing the MHD system in (1) introduces discretization errors that violate the divergence free condition (3) and thus simulates some unphysical behavior.

3 Galerkin Finite Element Method

To construct a finite element approximation we first define the mesh $\mathcal{T}_h$ of a domain Ω consisting of N triangles K. Then we define the finite element space

$$\mathcal{Q}_h = \{v \in C^0(\Omega); \forall K \in \mathcal{T}_h, v \in \mathbb{P}_k\},$$

where $\mathbb{P}_k$ is the space of polynomials of degree k, and $C^0(\Omega)$ is the space of continuous functions on Ω. Further we define the vector spaces $\boldsymbol{\mathcal{V}}_h = \mathcal{Q}^d$ and $\boldsymbol{\mathcal{W}}_h = \mathcal{Q}_h \times \boldsymbol{\mathcal{V}}_h \times \mathcal{Q}_h \times \boldsymbol{\mathcal{V}}_h$. The finite element approximation is then as follows: Find $\mathbf{U}_h(t) = [\rho_h,\ \mathbf{m}_h,\ E_h,\ \mathbf{B}_h]^T \in \boldsymbol{\mathcal{W}}_h$ such that

$$(\partial_t \mathbf{U}_h,\ \mathbf{V}_h) + (\nabla \cdot \mathbf{F}_\varepsilon(\mathbf{U}_h),\ \mathbf{V}_h) + (\nabla \cdot \mathbf{F}_\mathcal{B}(\mathbf{U}_h),\ \mathbf{V}_h) = \mathbf{0} \quad \forall\, \mathbf{V}_h \in \boldsymbol{\mathcal{W}}_h.$$

However, this straight-forward FEM approximation is not suitable for cases containing discontinuities or shocks, where a scheme like this would give rise to spurious oscillations. To address this issue, the monolithic

regularization term

$$\mathbf{F}_\nu := \begin{bmatrix} \epsilon\nabla\rho \\ \epsilon\nabla\mathbf{m} \\ \epsilon\nabla E \\ \epsilon\nabla\mathbf{B} \end{bmatrix},$$

introduced in [6] is added to the ideal MHD-equations, forming the monolithic flux MHD equations:

$$\partial_t\mathbf{U} + \nabla\cdot\mathbf{F}_\varepsilon(\mathbf{U}) + \nabla\cdot\mathbf{F}_\mathcal{B}(\mathbf{U}) - \nabla\cdot\mathbf{F}_\nu(\mathbf{U}) = \mathbf{0}.$$

This leads to the following stable finite element approximation: Find $\mathbf{U}_h(t) = [\rho_h, \mathbf{m}_h, E_h, \mathbf{B}_h]^T \in \boldsymbol{\mathcal{W}}_h$ such that

$$(\partial_t\mathbf{U}_h, \mathbf{V}_h) + (\nabla\cdot\mathbf{F}_\varepsilon(\mathbf{U}_h), \mathbf{V}_h) + (\nabla\cdot\mathbf{F}_\mathcal{B}(\mathbf{U}_h), \mathbf{V}_h) + (\mathbf{F}_\nu(\mathbf{U}_h), \nabla\mathbf{V}_h) \\ - (\mathbf{n}\cdot\mathbf{F}_\nu(\mathbf{U}_h), \mathbf{V}_h)_{\partial\Omega} = \mathbf{0} \quad \forall\, \mathbf{V}_h \in \boldsymbol{\mathcal{W}}_h, \quad (4)$$

where $\mathbf{n}$ is the normal vector defined on the boundary nodes. It is important that as we refine the mesh the monolithic flux MHD discretization converge to the straight-forward FEM discretization. Therefore, ϵ in the monolithic flux is chosen such that it tends to zero as h goes to zero.

3.1 Taylor-Hood Element

Discretizing the MHD equations using FEM with Generalized Lagrange Multipliers (GLM) or Artificial Compressibility (AC) results in the need of solving saddle-point like linear systems involving ψ, which are often ill-posed using irreducible/primal FEM. Therefore, special finite element spaces have been introduced, different for the different unknowns, referred to as mixed FEM. These discretizations ensure that the discrete, so called Ladyzhenskaya-Babuška-Brezzi (LBB) condition, or more often called the discrete 'inf-sup' condition, holds which is necessary to ensure that the discrete problem is well-posed. Inf-sup helps determining the ratio between degrees of freedom of two coupled quantities[11].

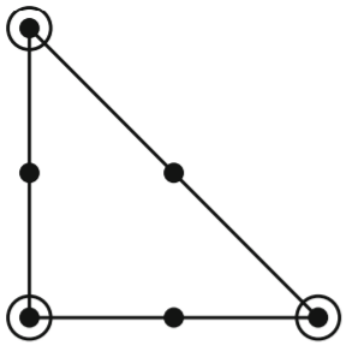

Figure 1: *Magnetic field* • *and scalar potential* ◯ *nodes for the* TH-*element.[11]*

The go to inf-sup stable element is the Taylor-Hood (TH) element[11], see Figure 1. TH-elements consists of continuous piecewise quadratic polynomials in space $\mathcal{V}_h$ and continuous piecewise linear polynomials in $\mathcal{Q}_h$ (the $\mathbb{P}_2 - \mathbb{P}_1$ pair).

3.2 Time Discretization

A strong stability-preserving (SSP) Runge Kutta 3 (RK3) [8] is used in this project to fully discretize the semi-discrete MHD problem. The discretization algorithm is presented in (5) and is an explicit third order

accurate method in time,

$$\begin{cases} \mathbf{U}^{n+1} = \mathbf{U}^n + \frac{1}{6}(k_1 + k_2 + 4k_3) \\ k_1 = h \cdot f\left(\mathbf{U}^n, t_n\right) \\ k_2 = h \cdot f\left(\mathbf{U}^n + h, t_n + k_1\right) \\ k_3 = h \cdot \left[f\left(\mathbf{U}^n + \frac{h}{4}, t_n + \frac{k_1}{2}\right) + f\left(\mathbf{U}^n + \frac{h}{4}, t_n + \frac{k_2}{2}\right)\right] \end{cases} \tag{5}$$

Since SSP RK3 is an explicit method, it is conditionally stable such that the time step must not violate the Courant–Friedrichs–Lewy (CFL) condition. The CFL-condition is presented in its generic form in (6). Here, v is the magnitude of the wave speed, Δt is the temporal step size and Δx is the spatial step size. This implies that when the spatial step size becomes smaller, the temporal step size needs to decrease as well in order to not violate the CFL-condition.

$$CFL = \frac{v\Delta t}{\Delta x} \leq C_{\max} \tag{6}$$

Applying the CFL-condition to the semi-discrete MHD-equations, the time step size δt has to obey the condition presented in (7) [5]. Here $\lambda_{\max}$ is the largest eigenvalue, which is presented in Section 2, and is thus the maximum wave speed, and $\min_{\mathbf{x}\in\Omega} h_h(\mathbf{x})$ is the smallest cell diameter.

$$\delta t = CFL \cdot \frac{\min_{\mathbf{x}\in\Omega} h_h(\mathbf{x})}{|\lambda^n_{\max,j}|}. \tag{7}$$

4 Divergence Cleaning Methods

4.1 Projection

A well known method of divergence cleaning is the Projection method, which is derived in [2]. The method projects the magnetic field, $\mathbf{B}$, onto a divergence-free space. This is done by introducing a new field $\mathbf{B}' = \mathbf{B} + \nabla\psi$, where ψ is the solution to the Poisson equation

$$\Delta\psi + \nabla \cdot \mathbf{B} = 0. \tag{8}$$

From (8) follows that the divergence of the magnetic field $\mathbf{B}'$ is zero:

$$\nabla \cdot (\nabla\psi + \mathbf{B}) = \nabla \cdot \mathbf{B}' = 0.$$

Solving for $\mathbf{B}'$ between each two consecutive time-steps and replacing $\mathbf{B}$ with $\mathbf{B}'$ would then satisfy the divergence free condition fully for each time-step. One drawback to this, otherwise simple method, is that solving the Poisson equation is considered costly in terms of computational time. Also, a finite element approximation of (8) is required for the implementation of the cleaning method.

4.2 Pseudo-Timestepping

Because of the high numerical cost of solving the Poisson equation at each time-step when using the Projection method, a different approach is proposed in [9] to solve the time-dependent equation

$$\partial_\tau\psi - \Delta\psi + \nabla \cdot B = 0, \tag{9}$$

instead of (8), which in equilibrium has the same solution. This scheme can be viewed as applying a numerically cheaper version of the Projection method several times. The time τ is a pseudo time, therein the name Pseudo-timestepping. The same methodology as in the Projection method is used for the Pseudo-timestepping method. Introduce the new field $\mathbf{B}' = \mathbf{B} + \nabla\psi$, where ψ is the solution to (9), and update the solver to use the field $\mathbf{B}'$. When implemented, the pseudo-timestepping is performed using a first order time-discretization

$$\frac{\psi^{n+1} - \psi^n}{\tau} - \Delta\psi^{n+1} + \nabla \cdot \mathbf{B}^n = 0.$$

4.3 Generalized Lagrange Multipliers

GLM is another way of imposing divergence cleaning introduced in [7]. This is done by replacing (1d) as well as the constraint in (3) by

$$\partial_t \mathbf{B} + \nabla \cdot (\mathbf{u} \otimes \mathbf{B} - \mathbf{B} \otimes \mathbf{u}) + \nabla \psi = 0,$$
$$\mathcal{D}(\psi) + \nabla \cdot \mathbf{B} = 0,$$

where $\mathcal{D}$ is a linear differential operator. Following the arguments made in [7], here the following choice is investigated,

$$\mathcal{D}(\psi) = \frac{1}{c_h^2}\partial_t \psi + \frac{1}{c_p^2}\psi,$$

which leads to the following divergence cleaning equations

$$\partial_t \mathbf{B} + \nabla \cdot (\mathbf{u} \otimes \mathbf{B} - \mathbf{B} \otimes \mathbf{u}) + \nabla \psi = 0, \tag{10a}$$
$$\partial_t \psi + c_h \nabla \cdot \mathbf{B} = -\frac{c_r c_h}{h}\psi. \tag{10b}$$

Here c_h is chosen as the maximum wave-speed given by the eigenvalues to the problem. c_r is the ratio $\frac{c_p^2}{c_h}$ and is set to be 0.3. The variable h is the mesh-size, which is given by the circumference of the elements. Given a sufficiently smooth solution it can be seen that this choice of the operator $\mathcal{D}$ leads to the telegraph equation for $\nabla \cdot \mathbf{B}$,

$$\partial_{tt}\left(\nabla \cdot \mathbf{B}\right) + \frac{c_h^2}{c_p^2}\partial_t\left(\nabla \cdot \mathbf{B}\right) - c_h^2 \Delta\left(\nabla \cdot \mathbf{B}\right) = 0.$$

This is a dissipative wave-equation, meaning that any errors in the divergence of the magnetic field are transported away from the source and dissipated. This implies that errors in the divergence cannot accumulate over time.

4.4 Artificial Compressibility

Adding one additional equation, one for the time derivative of an artificial potential function ψ, to the MHD-system of equations (1a-d) and modifying (1d) by the addition of the divergence of ψ, we obtain

$$\partial_t \mathbf{B} + \nabla \cdot (\mathbf{u} \otimes \mathbf{B} - \mathbf{B} \otimes \mathbf{u}) + \nabla \psi = 0, \tag{11a}$$
$$\epsilon \partial_t \psi + \nabla \cdot \mathbf{B} = 0 \iff \partial_t \psi + \lambda_{AC} \nabla \cdot \mathbf{B} = 0. \tag{11b}$$

In this way the ideal MHD equations have been modified similar to what is proposed by Chorin's AC method[4], for incompressible flows. The idea lies in the introduction of an artificial compressibility ϵ introduced to regularize the importance of the divergence free constraint. (11b) has been modified to use the penalty parameter $\lambda_{AC} = 1/\epsilon$ in accordance to [12]. The choice of the parameter λ_{AC} is important as it makes the problem stiffer the larger it is. The choice of suitable λ_{AC} is investigated in this report.

4.5 Grad-Div Stabilization

Grad-div stabilization (GD) is achieved by adding $-\epsilon\nabla(\nabla \cdot \mathbf{B})$ to the left hand side of (1d). In the finite element scheme, this yields a penalization term $\epsilon(\nabla \cdot \mathbf{B}_h, \nabla \cdot \mathbf{v}_h)$ that penalizes any discretization error that violates the divergence free condition (3). It has been shown that for approximate solutions to the Navier-Stokes equation with the use of GD using TH-element converge to pointwise divergence free solutions as $\epsilon \to \infty$ [3]. However, large ϵ increases the stiffness of the system leading to stability problems for explicit time-stepping methods. It is worthwhile noting that GD can be used in conjunction with the other methods in this project, however, it is here only applied together with the AC method.

5 Numerical Benchmarks

5.1 Smooth Vortex Problem[15]

To ensure that the divergence [15]cleaning methods do not destroy the convergence rate of the discretization error, these are implemented for a time-dependent smooth vortex problem with known solution [5]. The vortex problem is solved in 2D on the square domain $\Omega = [-10,\ 10] \times [-10,\ 10]$ for times $t \in [0,\ 0.05]$ with periodic boundary conditions on all boundaries, using a structured mesh.

The analytical solution reads

$$\big(\rho(t),\ \mathbf{u}(t),\ p(t),\ \mathbf{B}(t)\big) = \big(\rho_0,\ \mathbf{u}_0 + \delta\mathbf{u},\ p_0 + \delta p,\ \mathbf{B}_0 + \delta\mathbf{B}\big), \tag{12}$$

with the variables given as

$$\begin{aligned} &p_0 = 1 \\ &\mathbf{u}_0 = (1,\ 1), && \delta\mathbf{u} = \frac{\mu}{\sqrt{2}\pi} e^{(1-r^2)/2}(-r_2,\ r_1), \\ &\rho_0 = 0, && \delta p = -\frac{\mu^2}{8\pi^2}(1+r^2)e^{1-r^2}, \\ &\mathbf{B}_0 = (0.1,\ 0.1), && \delta\mathbf{B} = \frac{\mu}{2\pi} e^{(1-r^2)/2}(-r_2,\ r_1). \end{aligned} \tag{13}$$

Here, r is the vortex radius given by $r = \sqrt{r_1^2 + r_2^2}$, where $(r_1,\ r_2) = (x,\ y) - \mathbf{u}_0 t$. The vortex strength is given by $\mu = 5.389489439$ and adiabatic constant is $\gamma = \frac{5}{3}$.

5.2 2D Orszag-Tang[13]

The Orszag-Tang problem is a common problem for testing MHD solvers. In the solution of the problem, shocks and shock interference give rise to high numerical divergence errors, making it a good problem for testing divergence cleaning methods. The Orszag-Tang benchmark is commonly performed using numerical MHD schemes in 2D up to time $t = 0.5$ and thus serves as a basis for comparisons of results. In 2D, the problem is solved on the square domain $\Omega = [0,\ 1] \times [0,\ 1]$ where a magnetically conducting fluid is initiated moving in a vortex motion described by the initial condition:

$$(\rho,\ \mathbf{u},\ p,\ \mathbf{B}) = \left(\frac{25}{36\pi},\ (-\sin(2\pi y),\ \sin(2\pi x)),\ \frac{5}{12\pi},\ \left(-\frac{\sin(2\pi y)}{\sqrt{4\pi}},\ \frac{\sin(4\pi x)}{\sqrt{4\pi}}\right)\right),$$

and the adiabatic constant is $\gamma = \frac{5}{3}$. Periodic boundary conditions are implemented on all boundaries using built in FEniCS functions. The problem is solved on a right skewed structured mesh.

5.3 Cylinder Flow

To further study the effect of the divergence cleaning methods and their capabilities, the MHD problem is solved on another domain with a different geometry. The problem is the flow in a duct containing a cylindrical obstruction. In real MHD applications such as fusion reactors, periodic boundary conditions are not applicable. Therefore, we use more realistic boundary conditions here.

The domain is $\Omega = [0,\ 1] \times [0,\ 0.41]$ containing a cylinder of radius 0.05 centered at $[0.15,\ 0.205]$, see Figure 2. The boundary conditions are the so-called slip conditions, meaning that the normal components of $\mathbf{u}$ and $\mathbf{B}$ on the upper and lower boundary are set to zero, as well as their respective normal component on the cylinder boundary. The left boundary, $x = 0$, is set as inflow, and the right boundary, $x = 1$, is set as outflow. Initial conditions were set to comprise of a uniform flow to the right with adiabatic constant parameter $\gamma = \frac{5}{3}$;

$$(\rho_0,\ \mathbf{u}_0,\ p_0,\ \mathbf{B}_0) = \Big(1.4,\ (3.0,\ 0),\ 1.0,\ (0.1,\ 0)\Big).$$

The magnetic field is directed with the flow.

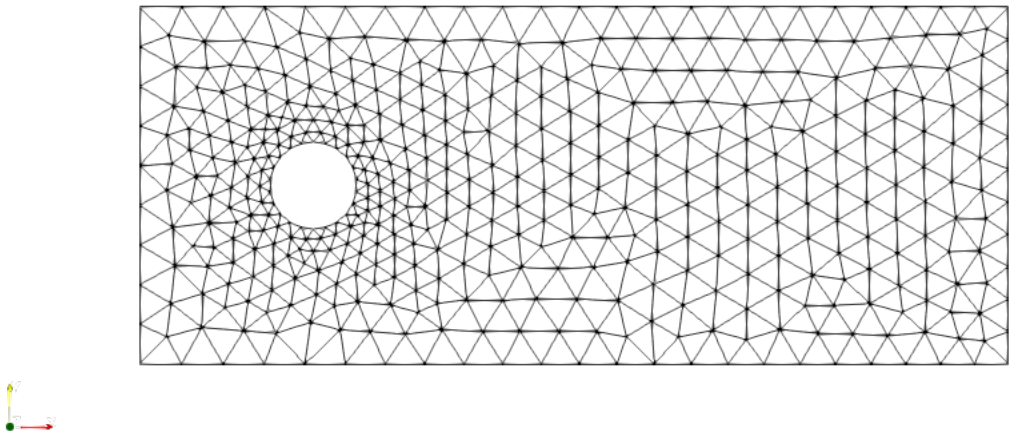

Figure 2: *Mesh of the cylinder benchmark.*

5.3.1 Boundary conditions

For the Projection and Pseudo-timestepping methods, boundary conditions had to be imposed for the quantity ψ in (8) and (9) respectively. Boundary conditions proved necessary where the magnetic field was not set, in this case the outflow boundary.

For the GLM and AC methods another approach was implemented. In the weak formulation of the methods, the term $(\nabla\psi, v) = -(\psi, \nabla \cdot \mathbf{V}) + (\psi, \mathbf{V})_{\partial\Omega}$ can be partially integrated obtaining boundary terms which set boundary conditions for the quantity ψ.

6 Results

6.1 Smooth Vortex Problem

All the presented cleaning methods were applied to the smooth vortex benchmark alongside using no cleaning as comparison. The convergence rates for the velocity solution $\mathbf{u}$ and the magnetic field solution $\mathbf{B}$ was calculated from the L^1- and L^2-residual norms, solving the problem with $\mathbb{P}_1$- and $\mathbb{P}_2$-discretization. For the AC-method, $\lambda_{AC} = 0.1$ was used through all discretizations, and for AC+GD, $\lambda_{AC} = 0.2$ was used. The results are presented in Tables 1-6, shown in Appendix A.

The L^2-convergence rates of the solutions are consistently around the correct order throughout all the studied divergence cleaning methods and discretization types. Overall, it can be seen that the solutions to the $\mathbb{P}_1$-discretization reaches a lower convergence rate to the solutions $\mathbf{u}$ and $\mathbf{B}$ than the expected theoretical quadratic convergence order $\mathcal{O}(h^2)$. Convergence rates of the solutions using $\mathbb{P}_2$- and TH-discretizations of about $\mathcal{O}(h^2) - \mathcal{O}(h^3)$ are also consistent with the theoretical cubic convergence rate. Cubic convergence being harder to reach in practice as a consequence of the nature of quadratic interpolators.
It is concluded that the Projection, Pseudo-timestepping, GLM, AC and AC+GD cleaning methods (with properly chosen parameter values) do not destroy the accuracy of the smooth vortex problem.

6.2 2D Orszag-Tang

In this section, Projection method, Pseudo-timestepping and GLM are implemented as divergence cleaning methods when solving the Orszag-Tang problem for $\mathbf{U}_h$. Then AC is implemented and a combination of AC with GD stabilization (AC+GD) for cleaning the $\mathbf{B}$-field when solving the Orszag-Tang problem.

Orszag-Tang is solved in 2D on different refined meshes and solved for times $T \in [0, 1]$ with fixed timestepping using RK3 and CFL-condition set to $CFL = 0.1$. The AC penalty parameter in (11b) is determined for the various refined meshes, we call this value '*critical* λ_{AC}' for the different meshes. Critical λ_{AC} is the parameter value for a specific mesh that will lead to AC (and AC+GD) best enforcing the divergence free constraint (3) (see Figure 4 in Appendix B using $\mathbb{P}_1$ elements) without making the problem to stiff to solve explicitly using the SSP RK3 scheme and the set CFL-condition.
A comparison based on the absolute divergence error $\int_\Omega |\nabla \cdot \mathbf{B}_h| d\mathbf{x}$ is then made between the methods.

6.2.1 $\mathbb{P}_1$ Discretization

The problem consisted of finding $\mathbf{U}_h \in \boldsymbol{\mathcal{W}}_h$ using no cleaning, Projection method, and Pseudo-timestepping and finding $\mathbf{U}_h \in \boldsymbol{\mathcal{W}}_h \times \boldsymbol{\mathcal{Q}}_h$, $k = 1$, using GLM, AC, and AC+GD. According to Figure 3 below, GLM and Projection method managed to reduce the absolute divergence error with Projection providing more intense cleaning. Pseudo-timestepping enforced the divergence free constraint more than Projection method at the expense of increasing computational time. Managing to best enforce the divergence free constraint is AC+GD followed by AC, both with proper choice of the penalty parameter λ_{AC}.

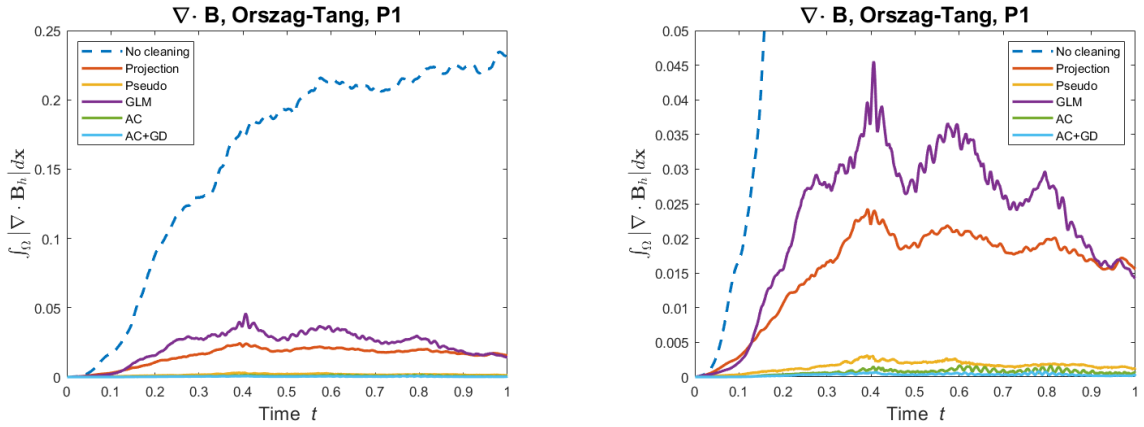

(a) $\mathbb{P}_1$, Absolute divergence error **(b)** Close-up

Figure 3: *Divergence error using $\mathbb{P}_1$-elements and Projection, Pseudo-timestepping, GLM, AC and AC+GD cleaning methods on the Orszag-Tang problem in 2D for $T \in [0, 1]$, $N = 60$, critical λ_{AC}*

The results for critical λ_{AC} implementing AC and AC+GD with $\mathbb{P}_1$-elements are presented in Table 7 and visualized in Figure 7. GD stabilization parameter $\epsilon = c_h h$ was used with c_h being the maximum wave speed. In Figure 7, critical λ_{AC} follows the mesh size h for both methods AC and AC+GD confirming the addition of AC cleaning stiffens the problem, and appropriate value of λ_{AC} has to be chosen. In addition, it is seen that by adding GD to AC, larger enforcement of the divergence free constraint is achieved and critical λ_{AC} increases.

Figure 4 presents the divergence error for the three choices of λ_{AC}, for the AC-method. Here, it was simulated for a grid size $N = 80$ together with $\mathbb{P}_1$-elements. The divergence cleaning results vary heavily between using the smaller $\lambda_{AC} = 0.05$ and the critical $\lambda_{AC} = 0.13$. If a larger λ_{AC} was used, the divergence error solution blew up. This demonstrates two aspects - a larger penalty parameter λ_{AC} reduces the divergence error but as an effect of increasing stiffness, could also violate the CFL-condition, requiring a smaller temporal step size, thus, increasing the cost of the simulation.

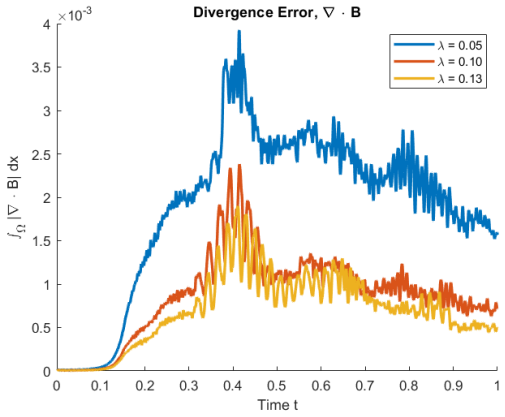

Figure 4: *Comparison of absolute divergence error solution to the Orszag-Tang problem in 2D implementing AC with different penalty parameter value λ_{AC}, $N = 80$. A larger λ_{AC} leads to smaller divergence error.*

6.2.2 $\mathbb{P}_2$ Discretization

Figure 5 shows how Pseudo-timestepping enforced the divergence free constraint more than the Projection method, which in turn enforced the divergence free constraint more than GLM. It also shows using AC with critical lambda achieves more cleaning than Pseudo-timestepping.

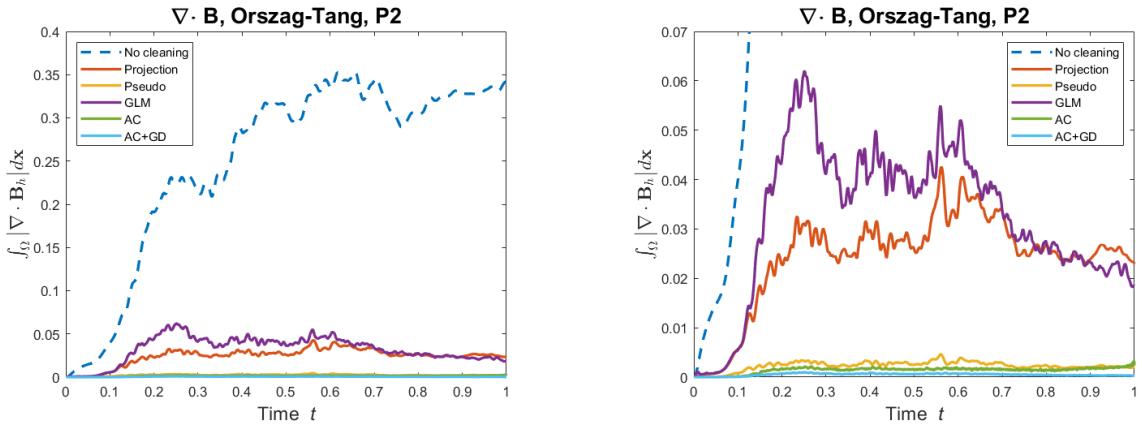

(a) $\mathbb{P}_2$, Absolute divergence error **(b)** Close-up

Figure 5: *Divergence error using $\mathbb{P}_2$-elements and Projection, Pseudo-timestepping, GLM, AC and AC+GD cleaning methods on the Orszag-Tang problem in 2D for $T \in [0, 1]$, $N = 60$, critical λ_{AC}*

The combination of using the methods AC and GD with $\epsilon = \frac{1}{2} c_h h$ further suppress the absolute divergence error. See the results in Table 8 (left) or Figure 7 showing critical λ_{AC} increasing as GD helps suppress spurious **B**-field divergence perturbations due to increased stiffness.

6.2.3 Taylor-Hood Discretization

In Figure 6 it can be seen that GLM, AC, and AC+GD methods all perform worse when implemented using TH-elements compared to using $\mathbb{P}_2$-elements In fact, using TH-elements, implementing GLM and implementing AC with critical λ_{AC} to solve Orszag-Tang yields almost identical solutions to the absolute divergence error seen as their respective solution is overlapping in Figure 6.

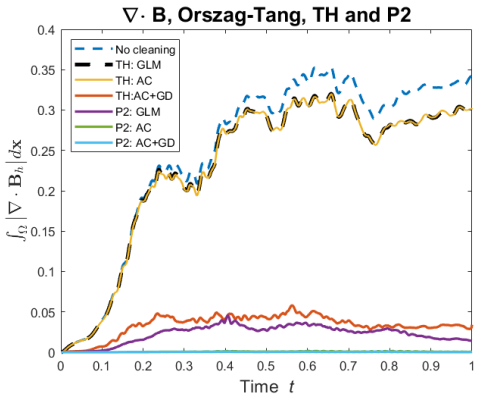

Figure 6: *Divergence error using TH-elements and Projection, Pseudo-timestepping, GLM, AC and AC+GD cleaning methods on the Orszag-Tang problem in 2D for* $T \in [0, 1]$, $N = 60$, *critical* λ_{AC}

The critical value of λ_{AC} is found for different refined meshes implementing AC and AC+GD with $\epsilon = \frac{1}{2} c_h h$. The results are presented in Table 8 (right column) and visualized in Figure 7. The results show that AC with TH-elements does not perform sufficient cleaning. In contrast, AC+GD perform much better, where the cleaning is mainly attributed to the GD cleaning part. Figure 6 shows potential in GD stabilization as a standalone cleaning method.

6.2.4 Summary

The Projection method and Pseudo-timestepping method work well to enforce the divergence free constraint. However, they quickly become computationally expensive on high resolution meshes using $\mathbb{P}_2$-elements. GLM, AC and AC+GD also perform the cleaning task well. AC, and AC+GD enforce the divergence free constraint more than GLM at the expense of the user having to choose penalty parameter λ_{AC}. Introducing an additional finite element space for ψ when using GLM and AC (and AC+GD) increases the computational cost of solving the problem and must be weighted against how well the methods enforce the divergence free constraint.

Based on Figure 7, a good assumption seems to be to choose the value of the critical λ_{AC}, up to some additive constant, linearly proportional and increase with the mesh-size h solving the Orszag-Tang problem in 2D for $T \in [0, 1]$. The mesh-size dependence holds true before and after adding GD to the AC divergence cleaning, and thus implies adding the AC method makes the problem stiffer for finer meshes. Adding GD stabilization increases the value of the critical λ_{AC} as an effect of GD penalizing spurious magnetic divergence perturbations that could turn into divergence blow-ups.

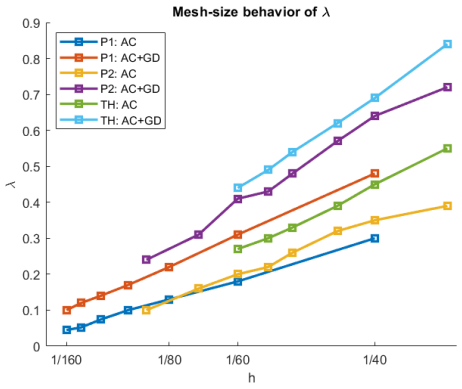

Figure 7: *Dependence on mesh-size of critical* λ_{AC} *using* $\mathbb{P}_1$-, $\mathbb{P}_2$-, TH *-elements and AC and AC+GD cleaning methods on the Orszag-Tang problem in 2D*

Figure 6 shows a poor divergence cleaning performance using GLM and AC. The inf-sup condition is assumed to be a necessary condition for a solution ψ to exist, this is clearly not the case as the MHD solver holds and cleaning is achieved using both equal order and mixed finite elements. In fact neither [7] or [4] developed GLM or AC for mixed finite elements such as using TH-elements. To explain the poor cleaning performance, it is suggested to start by examining if a different choice of parameter values in (10) and (11) could improve cleaning.

It is seen that at times $t \approx 0.3$, $t \approx 0.7$ and $t \approx 1.0$ the Orszag-Tang equation gets increasingly stiff as numerical solutions experienced divergence blow-ups, see Figure 10 in Appendix B using $\mathbb{P}_2$- and TH-elements. This can be related to complex shock collisions with the first pressure waves colliding around $t \approx 0.3$, more shocks are created at $t \approx 0.7$ and the flow is considered fully turbulent by $t \approx 1.0$.

Since the aim of this study does not concern the choice of GD parameter ϵ, finding a parameter value providing the most divergence cleaning has not been studied. Results from Jenkins et al. [10] on the Navier-Stokes equation points to the GD stabilization parameter ϵ not necessarily having to be chosen optimally to be $\mathcal{O}(1)$ as is widely accepted, but instead depends on multiple factors, two being the mesh size and the discretization method. Our testing showed that $\epsilon = \frac{1}{k} c_h h$ worked well, with k being the degree of the polynomial interpolator (1 and 2).

6.3 Cylinder Flow

In Figure 8 we show the absolute divergence error of the magnetic field as a function of time using the different cleaning methods for the cylinder flow test case. The simulation uses the mesh shown in Figure 2 and is discretized using $\mathbb{P}_1$-elements. Figure 8 shows that all the methods work well in reducing the divergence errors and keeping the error from increasing as it does without divergence cleaning. The best method is AC+GD. The worst method is the GLM method. The initial increase in the divergence error for the GLM, AC, and AC+GD is thought to be because of the inconsistent initial data, creating large amounts of divergence around the cylinder for the first few time-steps. For the Projection and Pseudo-timestepping methods a sharp initial decrease in divergence error is observed, as these two methods are applied separate from the MHD solving process, they might be seen to help fix the initial inconsistencies. For this benchmark not very large values of λ_{AC} have been tested. A functional λ_{AC} is instead chosen for the grid. The values $\lambda_{AC} = 0.1$ for the plain AC and $\lambda_{AC} = 0.15$ for AC+GD is chosen.

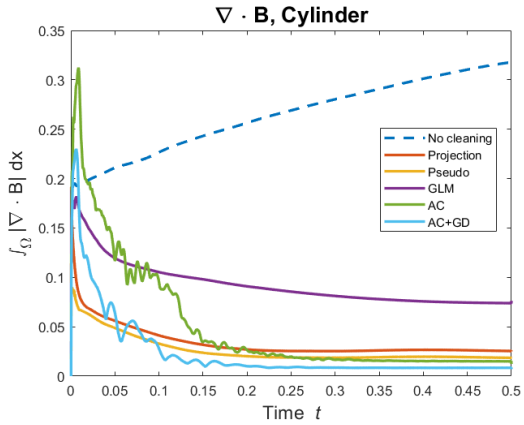

Figure 8: *Absolute divergence error over time for the cylinder problem using $\mathbb{P}_1$-elements for the different divergence cleaning methods.*

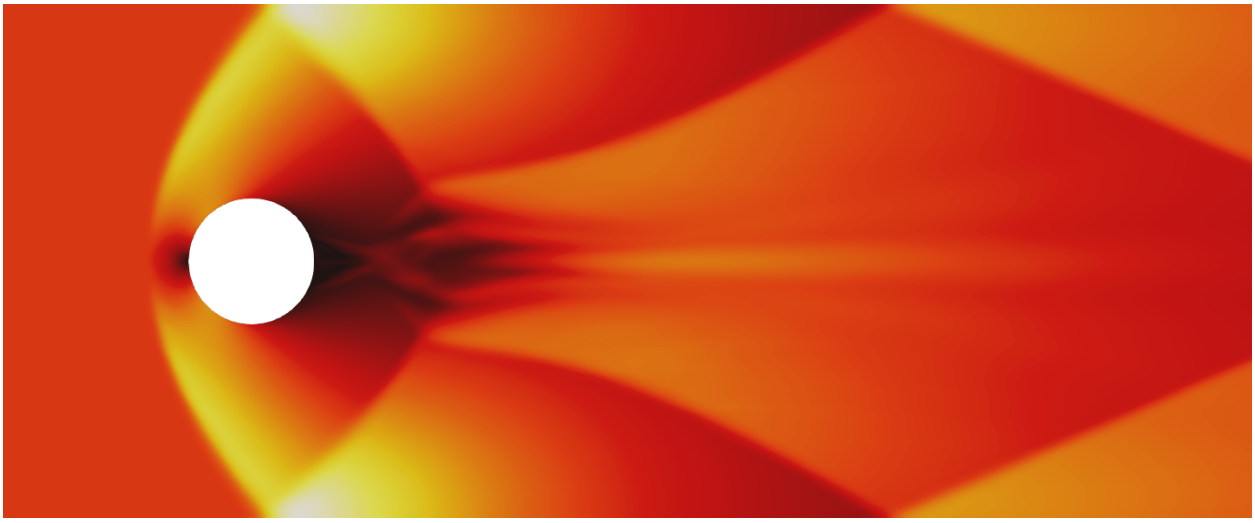

Figure 9: *The numerically computed* B*-field at time T=0.5 for the Cylinder problem with 35313* $\mathbb{P}^1$ *nodes using the projection method.*

7 Conclusions

The implemented divergence cleaning methods proved to be able to keep the divergence bounded for both the Orszag-Tang and the Cylinder flow problem. Our numerical experiments on the smooth vortex problem showed that none of the methods destroy the expected rates of convergence of the solution. Comparing the absolute divergence errors using the different divergence cleaning methods when solving the Orszag-Tang and Cylinder problem, showed that using AC+GD best enforced the divergence free constraint. Contrary to our first intuitions, the use of TH-elements to satisfy the discrete inf-sup condition worsened the divergence cleaning for the GLM and AC methods.

In this project, no analysis has been performed to study the necessity of fulfilling the discrete inf-sup condition between ψ and $\mathbf{B}$. As neither [7] or [4] developed GLM and AC using mixed FEM, further investigation regarding that may be required. Further studies can use Nédélec elements, that are point-wise divergence free. Using implicit time schemes could also introduce better divergence cleaning due to the high stiffness of the problem when using AC.

Acknowledgments

We would like to thank our supervisors Tuan Anh Dao and Lukas Lundgren for great guidance throughout this project and providing the code-package FEniCS_MHD_Solver. Their help is hereby gratefully acknowledged.

References

[1] Hannes Alfvén. *Facts - NobelPrize.org*. Nobel Prize Outreach AB. Jan. 16, 2022. URL: https://www.nobelprize.org/prizes/physics/1970/alfven/facts/.

[2] J.U Brackbill and D.C Barnes. "The Effect of Nonzero $\nabla \cdot B$ on the numerical solution of the magnetohydrodynamic equations". In: *Journal of Computational Physics* 35.3 (1980), pp. 426–430. ISSN: 0021-9991. DOI: https://doi.org/10.1016/0021-9991(80)90079-0. URL: https://www.sciencedirect.com/science/article/pii/0021999180900790.

[3] Michael Case et al. "A Connection Between Scott–Vogelius and Grad-Div Stabilized Taylor–Hood FE Approximations of the Navier–Stokes Equations". In: *SIAM J. Numerical Analysis* 49 (Jan. 2011), pp. 1461–1481. DOI: 10.2307/23074341.

[4] Alexandre Joel Chorin. "A Numerical Method for Solving Incompressible Viscous Flow Problems". In: *Journal of Computational Physics* 135.2 (1997), pp. 118–125. ISSN: 0021-9991. DOI: https://doi.org/10.1006/jcph.1997.5716. URL: https://www.sciencedirect.com/science/article/pii/S0021999197957168.

[5] Tuan Ahn Dao and Murtazo Nazarov. "A high-order residual-based viscosity finite element method for the ideal MHD equations". In: *(Preprint)* ().

[6] Tuan Ahn Dao and Murtazo Nazarov. "Monolithic parabolic regularization of the MHD equations and entropy principles". In: *(Preprint)* ().

[7] A. Dedner et al. "Hyperbolic Divergence Cleaning for the MHD Equations". In: *Journal of Computational Physics* 175.2 (2002), pp. 645–673. ISSN: 0021-9991. DOI: https://doi.org/10.1006/jcph.2001.6961. URL: https://www.sciencedirect.com/science/article/pii/S002199910196961X.

[8] Sigal Gottlieb, Chi-Wang Shu, and Eitan Tadmor. "Strong Stability-Preserving High-Order Time Discretization Methods". In: *SIAM Review* 43.1 (2001), pp. 89–112. ISSN: 00361445. URL: http://www.jstor.org/stable/3649684.

[9] Keiji Hayashi. "Magnetohydrodynamic Simulations of the Solar Corona and Solar Wind Using a Boundary Treatment to Limit Solar Wind Mass Flux". In: *The Astrophysical Journal Supplement Series* 161.2 (Dec. 2005), pp. 480–494. DOI: 10.1086/491791. URL: https://doi.org/10.1086/491791.

[10] Eleanor W. Jenkins et al. "On the parameter choice in grad-div stabilization for the Stokes equations". In: *Advances in Computational Mathematics* 40 (2014). ISSN: 1572-9044. DOI: https://doi.org/10.1007/s10444-013-9316-1. URL: https://link.springer.com/article/10.1007/s10444-013-9316-1.

[11] Mats G. Larson and Fredrik Bengzon. *The Finite Element Method: Theory, Implementation, and Applications*. Texts in Computational Science and Engineering, volume 10. Springer Heidelberg New York Dordrecht London, 2013. ISBN: 978-3-642-33286-9. DOI: 10.1007/978-3-642-33287-6.

[12] Lukas Lundgren and Murtazo Nazarov. "A high-order finite element method for incompressible variable density flow". In: *(Preprint)* ().

[13] Steven Alan Orszag and Cha-Mei Tang. "Small-scale structure of two-dimensional magnetohydrodynamic turbulence". In: *Journal of Fluid mechanics* 90.1 (1979), pp. 129–143. DOI: https://doi.org/10.1017/S002211207900210X. URL: https://doi.org/10.1006/10.1017/S002211207900210X.

[14] Kenneth G. Powell et al. "A Solution-Adaptive Upwind Scheme for Ideal Magnetohydrodynamics". In: *Journal of Computational Physics* 154.2 (1999), pp. 284–309. ISSN: 0021-9991. DOI: https://doi.org/10.1006/jcph.1999.6299. URL: https://www.sciencedirect.com/science/article/pii/S002199919996299X.

[15] Kailiang Wu and Chi-Wang Shu. "A provably positive discontinuous Galerkin method for multidimensional ideal magnetohydrodynamics". In: *SIAM J. Sci. Comput.* 40.5 (2018), B1302–B1329. DOI: https://doi.org/10.1137/18M1168042. URL: https://doi.org/10.1137/18M1168042.

Appendix A - Convergence Tables: Smooth Vortex Problem

Table 1: *L^1- and L^2-error and convergence rates for velocity* **u** *and magnetic field* **B** *using $\mathbb{P}_1$- and $\mathbb{P}_2$-elements without any implemented cleaning method.*

$\mathbb{P}_1$ discretization									
	u					**B**			
#DOFs	L^1-error	Rate	L^2-error	Rate	#DOFs	L^1-error	Rate	L^2-error	Rate
800	5.77E-03	-	3.01E-02	-	882	2.31E-01	-	2.42E-01	-
3200	1.61E-03	1.85	9.11E-03	1.72	3362	6.41E-02	1.91	7.31E-02	1.79
12800	3.80E-04	2.08	2.14E-03	2.09	13122	1.51E-02	2.12	1.71E-02	2.13
51200	8.98E-05	2.08	5.01E-04	2.09	51842	3.58E-03	2.10	4.01E-03	2.11
$\mathbb{P}_2$ discretization									
	u					**B**			
#DOFs	L^1-error	Rate	L^2-error	Rate	#DOFs	L^1-error	Rate	L^2-error	Rate
3200	7.15E-04	-	4.28E-03	-	3362	2.86E-02	-	3.41E-02	-
12800	9.32E-05	2.94	5.61E-04	2.93	13122	3.91E-03	2.92	4.47E-03	2.99
51200	1.86E-05	2.33	1.10E-04	2.35	51842	7.58E-04	2.39	8.30E-04	2.45

Table 2: *L^1- and L^2-error and convergence rates for velocity* **u** *and magnetic field* **B** *using $\mathbb{P}_1$- and $\mathbb{P}_2$-elements with the Projection method.*

$\mathbb{P}_1$ discretization									
	u					**B**			
#DOFs	L^1-error	Rate	L^2-error	Rate	#DOFs	L^1-error	Rate	L^2-error	Rate
800	5.77E-03	-	3.01E-02	-	882	2.39E-01	-	2.43E-01	-
3200	1.61E-03	1.85	9.11E-03	1.72	3362	6.44E-02	1.96	7.31E-02	1.79
12800	3.80E-04	2.08	2.14E-03	2.09	13122	1.52E-02	2.12	1.71E-02	2.13
51200	8.98E-05	2.08	5.01E-04	2.09	51842	3.58E-03	2.10	4.01E-03	2.11
$\mathbb{P}_2$ discretization									
	u					**B**			
#DOFs	L^1-error	Rate	L^2-error	Rate	#DOFs	L^1-error	Rate	L^2-error	Rate
3200	7.75E-04	-	4.69E-03	-	3362	3.25E-02	-	3.66E-02	-
12800	9.35E-05	3.05	5.61E-04	3.06	13122	4.26E-03	2.98	4.46E-03	3.09
51200	1.84E-05	2.34	1.10E-04	2.36	51842	8.31E-04	2.38	8.46E-04	2.42

Table 3: *L^1- and L^2-error and convergence rates for velocity* $\mathbf{u}$ *and magnetic field* $\mathbf{B}$ *using* $\mathbb{P}_1$- *and* $\mathbb{P}_2$*-elements with Pseudo-timestepping method.*

$\mathbb{P}_1$ discretization									
	u					**B**			
#DOFs	L^1-error	Rate	L^2-error	Rate	#DOFs	L^1-error	Rate	L^2-error	Rate
800	5.77E-03	-	3.01E-02	-	882	2.47E-01	-	2.44E-01	-
3200	1.61E-03	1.85	9.11E-03	1.72	3362	6.47E-02	2.00	7.31E-02	1.80
12800	3.80E-04	2.08	2.14E-03	2.09	13122	1.52E-02	2.13	1.71E-02	2.13
51200	8.98E-05	2.08	5.01E-04	2.09	51842	3.58E-03	2.10	4.01E-03	2.11
$\mathbb{P}_2$ discretization									
	u					**B**			
#DOFs	L^1-error	Rate	L^2-error	Rate	#DOFs	L^1-error	Rate	L^2-error	Rate
3200	7.69E-04	-	4.61E-03	-	3362	3.46E-02	-	3.61E-02	-
12800	9.45E-05	3.02	5.67E-04	3.02	13122	4.88E-03	2.88	4.55E-03	3.04
51200	1.85E-05	2.36	1.10E-04	2.37	51842	9.77E-04	2.34	8.71E-04	2.41

Table 4: *L^1- and L^2-error and convergence rates for velocity* $\mathbf{u}$ *and magnetic field* $\mathbf{B}$ *using* $\mathbb{P}_1-, \mathbb{P}_2$- *and* TH*-elements with the GLM method.*

$\mathbb{P}_1$ discretization									
	u					**B**			
#DOFs	L^1-error	Rate	L^2-error	Rate	#DOFs	L^1-error	Rate	L^2-error	Rate
800	5.77E-03	-	3.01E-02	-	882	2.31E-01	-	2.42E-01	-
3200	1.61E-03	1.85	9.11E-03	1.72	3362	6.41E-02	1.91	7.31E-02	1.57
12800	3.80E-04	2.08	2.14E-03	2.09	13122	1.51E-02	2.12	1.71E-02	2.11
51200	8.98E-05	2.08	5.01E-04	2.09	51842	3.58E-03	2.10	4.01E-03	2.16
$\mathbb{P}_2$ discretization									
	u					**B**			
#DOFs	L^1-error	Rate	L^2-error	Rate	#DOFs	L^1-error	Rate	L^2-error	Rate
3200	7.16E-04	-	4.28E-03	-	3362	2.82E-02	-	3.35E-02	-
12800	9.30E-05	2.94	5.58E-04	2.94	13122	3.99E-03	2.87	4.39E-03	2.99
51200	1.83E-05	2.34	1.09E-04	2.36	51842	8.54E-04	2.24	8.96E-04	2.31
TH discretization									
	u					**B**			
#DOFs	L^1-error	Rate	L^2-error	Rate	#DOFs	L^1-error	Rate	L^2-error	Rate
3200	7.15E-04	-	4.28E-03	-	3362	2.85E-02	-	3.41E-02	-
12800	9.32E-05	2.94	5.61E-04	2.93	13122	3.91E-03	2.92	4.47E-03	2.99
51200	1.86E-05	2.33	1.10E-04	2.35	51842	7.58E-04	2.39	8.30E-04	2.45

Table 5: *L^1- and L^2-error and convergence rates for velocity* $\mathbf{u}$ *and magnetic field* $\mathbf{B}$ *using* $\mathbb{P}_1-, \mathbb{P}_2$- *and* TH-*elements with the AC method,* $\lambda_{AC} = 0.1$.

$\mathbb{P}_1$ discretization									
	u					**B**			
#DOFs	L^1-error	Rate	L^2-error	Rate	#DOFs	L^1-error	Rate	L^2-error	Rate
800	5.77E-03	-	3.01E-02	-	882	2.31E-01	-	2.42E-01	-
3200	1.61E-03	1.85	9.11E-03	1.72	3362	6.41E-02	1.91	7.31E-02	1.79
12800	3.80E-04	2.08	2.14E-03	2.09	13122	1.52E-02	2.12	1.71E-02	2.13
51200	8.98E-05	2.08	5.01E-04	2.09	51842	3.58E-03	2.10	4.01E-03	2.11
$\mathbb{P}_2$ discretization									
	u					**B**			
#DOFs	L^1-error	Rate	L^2-error	Rate	#DOFs	L^1-error	Rate	L^2-error	Rate
3200	7.15E-04	-	4.28E-03	-	3362	2.83E-02	-	3.38E-02	-
12800	9.31E-05	2.94	5.60E-04	2.93	13122	3.93E-03	2.90	4.38E-03	3.00
51200	1.84E-05	2.34	1.10E-04	2.35	51842	1.09E-03	1.87	1.06E-04	2.06
TH discretization									
	u					**B**			
#DOFs	L^1-error	Rate	L^2-error	Rate	#DOFs	L^1-error	Rate	L^2-error	Rate
3200	7.15E-04	-	4.28E-03	-	3362	2.85E-02	-	3.41E-02	-
12800	9.32E-05	2.94	5.61E-04	2.93	13122	3.91E-03	2.92	4.47E-03	2.99
51200	1.86E-05	2.33	1.10E-04	2.35	51842	7.58E-04	2.39	8.29E-04	2.45

Table 6: *L^1- and L^2-error and convergence rates for velocity* $\mathbf{u}$ *and magnetic field* $\mathbf{B}$ *using* $\mathbb{P}_1-, \mathbb{P}_2$- *and* TH-*elements with AC+GD method,* $\lambda_{AC} = 0.2$.

$\mathbb{P}_1$ discretization									
	solution $\mathbf{u}$					solution $\mathbf{B}$			
#DOFs	L^1-error	Rate	L^2-error	Rate	#DOFs	L^1-error	Rate	L^2-error	Rate
800	5.77E-03	-	3.01E-02	-	882	2.67E-01	-	2.70E-01	-
3200	1.61E-03	1.85	9.11E-03	1.72	3362	6.90E-02	2.02	7.89E-02	1.84
12800	3.80E-04	2.08	2.14E-03	2.09	13122	1.57E-02	2.18	1.79E-02	2.18
$\mathbb{P}_2$ discretization									
	solution $\mathbf{u}$					solution $\mathbf{B}$			
#DOFs	L^1-error	Rate	L^2-error	Rate	#DOFs	L^1-error	Rate	L^2-error	Rate
3200	7.16E-04	-	4.29E-03	-	3362	3.17E-02	-	3.44E-02	-
12800	9.30E-05	2.94	5.60E-04	2.94	13122	4.33E-02	2.92	4.52E-03	2.98
51200	1.84E-05	2.33	1.10E-04	2.35	51842	8.93E-04	2.30	9.13E-04	2.33
TH discretization									
	solution $\mathbf{u}$					solution $\mathbf{B}$			
#DOFs	L^1-error	Rate	L^2-error	Rate	#DOFs	L^1-error	Rate	L^2-error	Rate
3200	7.15E-04	-	4.29E-03	-	3362	3.16E-02	-	3.45E-02	-
12800	9.30E-05	2.94	5.60E-04	2.94	13122	4.22E-03	2.96	4.49E-03	2.99
51200	1.85E-05	2.33	1.10E-04	2.35	51842	7.93E-04	2.44	8.46E-04	2.43

Appendix B

Table 7: *Critical values of λ_{AC} for different mesh sizes N using $\mathbb{P}_1$-elements on the Orszag-Tang problem in 2D solved for times $T \in [0,1]$, implementing the AC and AC+GD cleaning methods with $\epsilon = c_h h$ and $CFL = 0.1$.*

N	AC	AC+GD
40	0.30	0.48
60	0.18	0.31
80	0.13	0.22
100	0.10	0.17
120	0.074	0.14
140	0.052	0.12
160	0.045	0.10

Table 8: *Critical values of λ_{AC} for different mesh sizes N using $\mathbb{P}_2$- and* TH*-elements on the Orszag-Tang problem in 2D solved for times $T \in [0,1]$, implementing the AC and AC+GD cleaning methods with $\epsilon = \frac{1}{2} c_h h$ and $CFL = 0.1$.*

	$\mathbb{P}_2$ element		TH element	
N	AC	AC+GD	AC	AC+GD
34	0.39	0.72	0.55	0.84
40	0.35	0.64	0.45	0.69
44	0.32	0.57	0.39	0.62
50	0.26	0.48	0.33	0.54
54	0.22	0.43	0.30	0.49
60	0.20	0.41	0.27	0.44
70	0.16	0.31	–	–
90	0.10	0.24	–	–

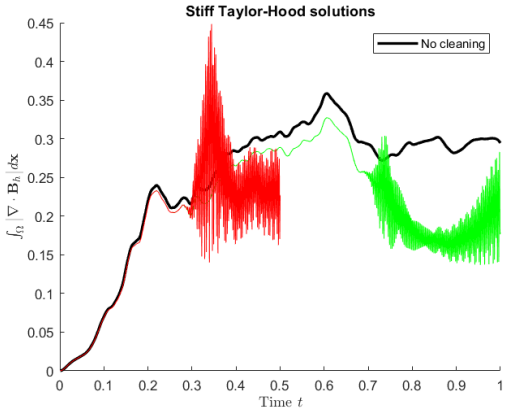

Figure 10: *Absolute divergence error over time using* TH*-elements and AC. Divergence blow-up (large amplitude rapid oscillations) due to complex shock capturing starting at $t \approx 0.3$ (red) and $t \approx 0.7$ not possible with penalty parameter λ_{AC} set too high*